Obrabotka metallov (tekhnologiya, oborudovanie, instrumenty) = Metal Working and Material Science. 2024 vol. 26 no. 3 pp. 286–297
ISSN: 1994-6309 (print) / 2541-819X (online)
DOI: 10.17212/1994-6309-2024-26.3-286-297

NSTU NETI

Obrabotka metallov - Metal Working and Material Science

Journal homepage: http://journals.nstu.ru/obrabotka_metallov

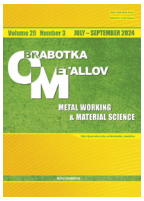

Fine structure features of Ni-Al coatings obtained by high velocity atmospheric plasma spraying

Elena Kornienko [1, a, *], ***Igor Gulyaev*** [2, b], ***Alexandr Smirnov*** [1, c], ***Natalya Plotnikova*** [1, d], ***Viktor Kuzmin*** [2, e], ***Valeriy Golovakhin*** [1, f], ***Alexandr Tambovtsev*** [2, g], ***Pavel Tyryshkin*** [2, h], ***Dmitry Sergachev*** [2, i]

[1] Novosibirsk State Technical University, 20 Prospekt K. Marksa, Novosibirsk, 630073, Russian Federation
[2] Khristianovich Institute of Theoretical and Applied Mechanics SB RAS, 4/1 Institutskaya str., Novosibirsk, 630090, Russian Federation

[a] https://orcid.org/0000-0002-5874-5422, e.kornienko@corp.nstu.ru; [b] https://orcid.org/0000-0001-5186-6793, gulyaev@itam.nsc.ru;
[c] https://orcid.org/0000-0003-3746-8793, micros20t@mail.ru; [d] https://orcid.org/0000-0002-8005-1128, n.plotnikova@corp.nstu.ru;
[e] https://orcid.org/0000-0002-9951-7821, vikuzmin57@mail.ru; [f] https://orcid.org/0000-0003-3396-8491, golovaxin-valera@mail.ru;
[g] https://orcid.org/0000-0003-1635-9352, alsetams@gmail.com; [h] https://orcid.org/0009-0009-8125-6772, pavel99730@gmail.com;
[i] https://orcid.org/0000-0003-2469-5946, dsergachev@itam.nsc.ru

ARTICLE INFO

Article history:
Received: 14 June 2024
Revised: 14 July 2024
Accepted: 07 August 2024
Available online: 15 September 2024

Keywords:
High velocity atmospheric plasma spraying
Coating
Ni-Al
HV-APS

Funding
The work was carried out within the framework of the state assignment of ITAM SB RAS.

Acknowledgements
The research was carried out on the equipment of the Collective Use Center "Structure, Mechanical and Physical Properties of Materials".

ABSTRACT

Introduction. Development of *Ni-Al* intermetallic compounds is one of the priority directions of modern machine building. Due to such characteristics as high heat resistance, high temperature strength, and low density, nickel aluminides are used as functional coatings in the aerospace industry. The main methods of *Ni-Al* coating surfacing are High-Velocity Oxygen-Fuel and High-Velocity Air-Fuel spraying (*HVOF* and *HVAF*), atmospheric plasma spraying (*APS*) and its modification such as High-Velocity Atmospheric Plasma spraying (*HV-APS*) which provides non-equilibrium cooling conditions. Since there are eight different intermetallic compounds, as well as martensite transformation, *Ni-Al* coatings is quite interesting to study. **The work purpose** is to study the features of the martensitic structure in *HV-APS* coatings, and also to establish the effect of heating temperature on its decomposition. **Materials and methods.** *Ni-Al* coatings were surfaced onto a low-carbon steel substrate using the *HV-APS* method. Studies of the fine structure of the coatings were carried out using transmission electron microscopy (*TEM*). In addition, the influence heating temperature on structural transformations of the coatings was analyzed. **Results and discussion.** Two types of particles are formed in *HV-APS* coatings: with a dendritic and granular structure. The most part of *HV-APS* coatings consists of particles with a two-phase grain structure (Ni_xAl_{1-x} and γ'-Ni_3Al grains). Only Ni_xAl_{1-x} grains undergo martensitic transformation at cooling. Martensite in large grains (sizes greater than 500 nm) has a lamellar structure, while small grains are completely transformed into one martensite plate. In addition, the coatings contain grains in which martensite plates (Ni_xAl_{1-x}) and β-phases alternated. It is shown the behavior of martensitic plates at colliding with each other, as well as with the γ'-Ni_3Al grain. Heating up to 400 °C contribute the begins of martensite decomposition in individual grains with the release of a secondary phase; after heating up to 600 °C all martensite dissolves.

For citation: Kornienko E.E., Gulyaev I.P., Smirnov A.I., Plotnikova N.V., Kuzmin V.I., Golovakhin V., Tambovtsev A.S., Tyryshkin P.A., Sergachev D.V. Fine structure features of Ni-Al coatings obtained by high velocity atmospheric plasma spraying. *Obrabotka metallov (tekhnologiya, oborudovanie, instrumenty) = Metal Working and Material Science*, 2024, vol. 26, no. 3, pp. 286–297. DOI: 10.17212/1994-6309-2024-26.3-286-297. (In Russian).

*** Corresponding author**
Kornienko Elena E., Ph.D. (Engineering), Associate Professor
Novosibirsk State Technical University,
20 Prospekt K. Marksa,
630073, Novosibirsk, Russian Federation
Tel.: +7 383 346-53-59, **e-mail:** e.kornienko@corp.nstu.ru

Introduction

Nowadays, intermetallic materials design for structural purposes is one of the priority areas for the development of modern mechanical engineering. Due to the combination of characteristics such as high heat resistance and thermal conductivity, the ability to maintain strength and rigidity at high temperatures and relatively low density [1–3], nickel aluminides are used as materials for components of aircraft engines, gas turbines and heat exchangers [4–6]. It is vital that *Ni-Al* system alloys, being high-temperature materials, have low ductility and fracture toughness at room temperature [6] and this limits its use as bulk parts. In turn, one of the solutions to this problem is the use of nickel aluminides as functional coatings. In general, the main methods of applying *Ni-Al* coatings are high-velocity oxygen-fuel spraying (*HVOF*) [7–9], high-velocity air-fuel spraying (*HVAF*) [9, 10], atmospheric plasma spraying (*APS*) [11–14] and also its modification such as high-velocity atmospheric plasma spraying (*HV-APS*).

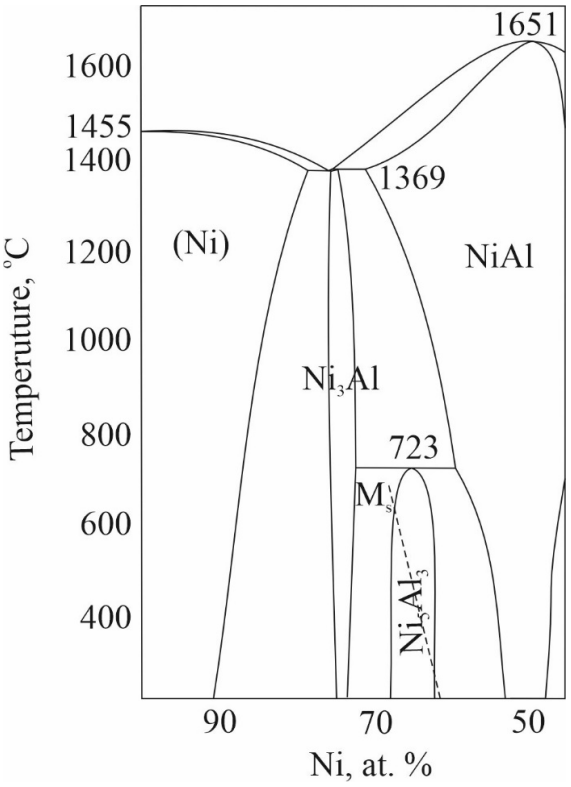

Fig. 1. Part of *Ni-Al* phase diagram

There are eight stable and metastable intermetallic compounds in the *Ni-Al* system [15], the most promising of which are aluminides located in the nickel-rich part of the phase diagram, such as γ′-Ni_3Al and β-*NiAl* (Fig. 1) [3, 16, 17]. β-*NiAl* solid solutions have a wide range of homogeneity (43–70 at. % *Ni* at 1,400 °C), which decreases to 45–60 at. % *Ni* at a room temperature [3, 16]. Cooling of the β-phase in the range of high *Ni* concentrations is accompanied by the formation of a mixture of β- and γ′-phases, while grains of the β-*NiAl* phase often have different chemical compositions. The martensitic transformation $\boldsymbol{B2 \rightarrow L1_0}$ occurs in β-phase crystals containing more than 62.3 at. % *Ni*. The onset temperature of this transformation ($\boldsymbol{M_s}$) varies, according to various sources, from −200 to ~ 650 or 900 °C [17–19] depending on the *Ni* concentration. Subsequent heating of alloys from 62.5–68.0 at. % *Ni* promotes the separation of the Ni_5Al_3 phase or the metastable Ni_2Al phase [20–22].

As a rule, coatings with a similar composition are often used as a bonding layer between the base material and a ceramic heat-shielding coating (*YSZ*) [23]. *Chen et al.* [24] discovered that the martensitic transformation occurring in the metal sublayer can cause the destruction of the ceramic coating due to changes in volume during the transformation of the β-phase into martensite. Thus, the study of the structural-phase state, as well as the understanding of structural transformations are priority tasks in the *Ni-Al* coatings design, since both functional and mechanical, as well as technological properties will depend on this.

The purpose of this work is to study the features of the martensitic structure of *Ni-Al* coatings obtained by the *HV-APS* method. To achieve this purpose, the following tasks were solved:

- study of the coatings structure;
- study of the features of the martensitic structure depending on the grain size;
- study of the behavior of martensitic plates when colliding with other structural components;
- study of the influence of heating temperature on the structure of the coatings.

Materials and methods

Ni-Al coatings 500–600 μm thick were spraying on discs from low carbon steel with a diameter of 20 mm and a thickness of 8 mm. The particle size of powder was 40–100 μm, chemical composition was 75 at. % *Ni* and 25 at. % *Al*. To apply the coatings, we used the *Termoplasma 50* plasma spraying installation,

equipped with an *HV-APS* plasma torch. The supersonic spraying mode using air as the working gas ensures the speed of the sprayed particles at a level of 500 m/s and higher. Optimal modes for high-velocity spraying *Ni-Al* powder are presented in our previous work [25].

To analyze the structural state of the coatings, a scanning electron microscope (*Carl Zeiss EVO50 XVP* with an *EDS X-Act* microanalyzer) and a transmission electron microscope (*FEI Tecnai G2 20 TWIN*) were used. Transverse sections of coatings were the samples for *SEM* as well as foils, cut from the middle of the coatings, were the samples for *TEM*.

Ni-Al coatings were kept for 1 hour at temperatures of 300, 400, 500 and 600 °C (air cooling) to study the structural transformations that occur upon heating.

Results and discussion

Previously, we have shown that *HV-APS* coatings are characterized by the presence of several zones that differ in structure [25]. Fig. 2 shows *SEM* image and scheme of the microstructure of the *HV-APS* coating in the initial state. The chemical composition of all areas was determined using micro-X-ray spectral analysis. According to the data obtained, there are particles, the central part of which is the β-*NiAl* intermetallic compound (section **1** in Fig. 2), surrounded by a single-phase layer of the β-*NiAl* phase enriched in *Ni* (referred to as the Ni_xAl_{1-x} phase) (section **2** in Fig. 2). The structure of section **3** in Fig. 2 is dendritic: the chemical composition of the dendrites coincides with the composition of the layer (section **2**), and the chemical composition of the interdendritic space corresponds to theγ'-Ni_3Al phase. We considered the fine structure of these areas more thoroughly in our work [25]. As a rule, the particles with a similar structure are not common for *HV-APS* coatings. Predominant particles are particles with two-phase structure consisting of Ni_xAl_{1-x} and γ'-Ni_3Al grains (section B in fig. 2).

Fig. 3 shows *TEM* images of section **4**. It can be seen that Ni_xAl_{1-x} grains undergo a shear martensitic transformation, during which the high-temperature ***B2*** structure transforms into the low-temperature $\boldsymbol{L1_0}$ structure, while the γ′-Ni_3Al grains do not change. There are also one-phase areas consisting only of grains of the γ′-Ni_3Al phase (fig. 3, *b*). The shape of the grains in section **4** is non-equiaxial, which is typical for material cooled under non-equilibrium conditions. The grain sizes usually do not exceed 500 nm, although sometimes larger γ′-Ni_3Al grains are formed. Such grains often have deformation twins (Fig. 3, *c*) and stacking faults (Fig. 3, *d*).

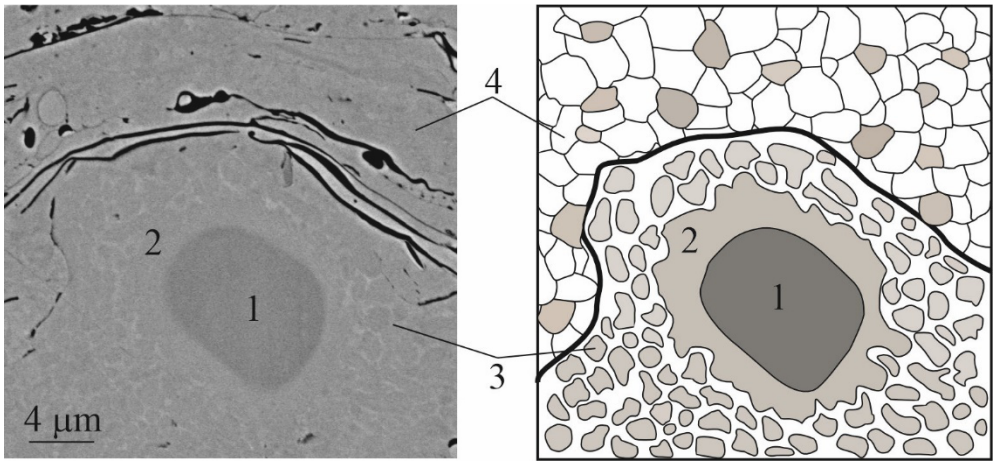

a *b*

Fig. 2. SEM image (*a*) and scheme (*b*) of *HV-APS* coatings:

1 – β-*NiAl* phase; ***2*** – layer of Ni_xAl_{1-x}; ***3*** – area with dendritic structure: Ni_xAl_{1-x} dendrites, interdendritic region (γ'-Ni_3Al phase); ***4*** – area with grain structure: both Ni_xAl_{1-x} and Ni_3Al grains

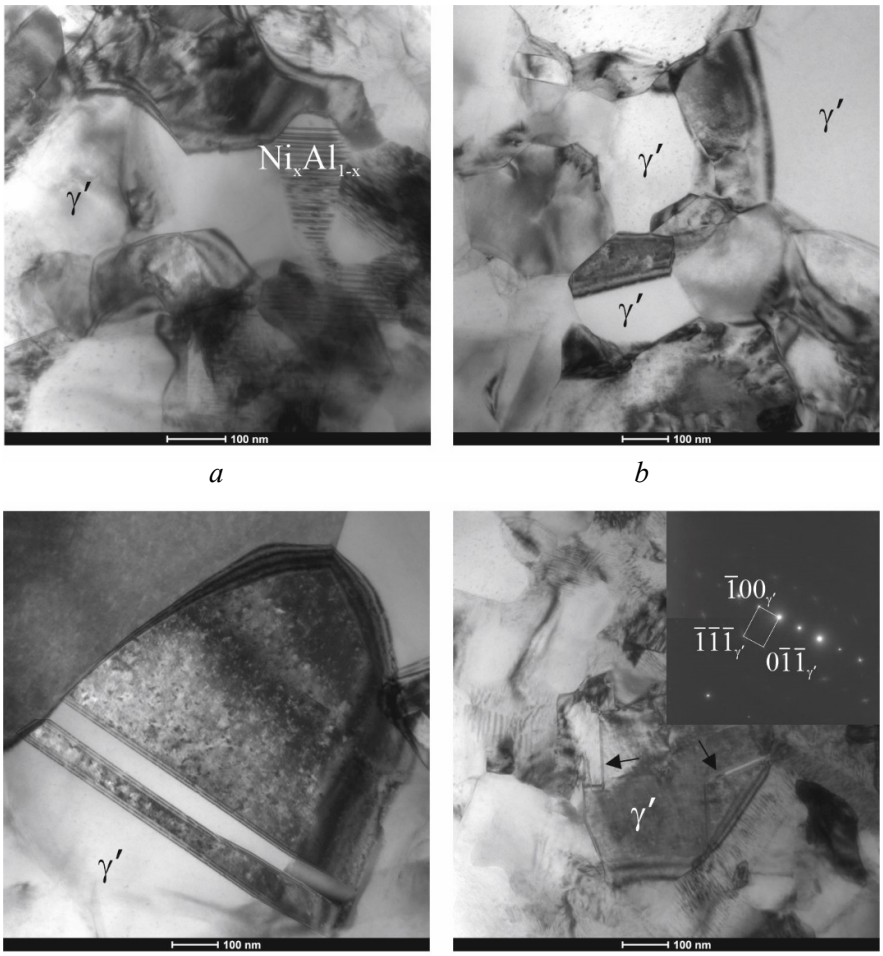

a *b*

c *d*

Fig. 3. Bright field *TEM* images of *HV-APS* coatings:
a – two-phase area of Ni_xAl_{1-x} + γ′-Ni_3Al; *b* – one-phase area of γ′-Ni_3Al; *c)* twins in γ′-Ni_3Al; *d* – stacking faults in γ′-Ni_3Al with diffraction pattern

Martensite in *HV-APS* coatings is lamellar (Fig. 4), but depending on the size of the grains in which the transformation occurs, it looks different. For example, martensite formed in large Ni_xAl_{1-x} grains consists of plates located in a twinned orientation relative to each other (Fig. 4, *a*). The distance between microtwins may be from 0.5 nm (Fig. 4, *b*) to several nanometers (fig. 4, *a*). The martensite-martensite interface can be located both inside the former Ni_xAl_{1-x} grain and outside it (Fig. 4, *c*). Unlike large grains (greater than 500 nm), fine grains completely transform into one microtwinning plate (Fig. 4, *d*). Sometimes there are martensitic grains in which, even with the use of a dark field, it is not possible to detect microtwins in pairs of parallel plates, and these plates appear to be single crystals (Fig. 5). According to data of local chemical analysis, adjacent plates have different chemical compositions. The *Ni* content in plates with microtwins (type **1**) is 77.4 at. %, which corresponds to the Ni_xAl_{1-x} phase, while the *Ni* content in plates without microtwins (type **2**) is 52.5 at. %, which corresponds to the β-phase.

Martensite plates can behave differently when collide with each other or with other phases. For example, growth of individual thin plates growing in different directions often does not stop. These plates pass through each other and only the area of its intersection is rearranged (Fig. 4, *a*). Fig. 6, *a*, *b* shows that when a martensitic plate collides with a γ′-Ni_3Al grain, it does not penetrate into it, but continues to transform. On the other hand, Fig. 6, *c* shows martensitic plates that seem to have grown inside the γ′-Ni_3Al grain. Apparently, in this case, the Ni_xAl_{1-x} plates appeared first, around which the γ′-Ni_3Al phase later formed. Some plates change the direction of its growth, deviating to the side at collision with obstacle (Fig. 6, *d*). Deformation and elastic distortions occur in areas near curved plates, which contrast is visible near the bend.

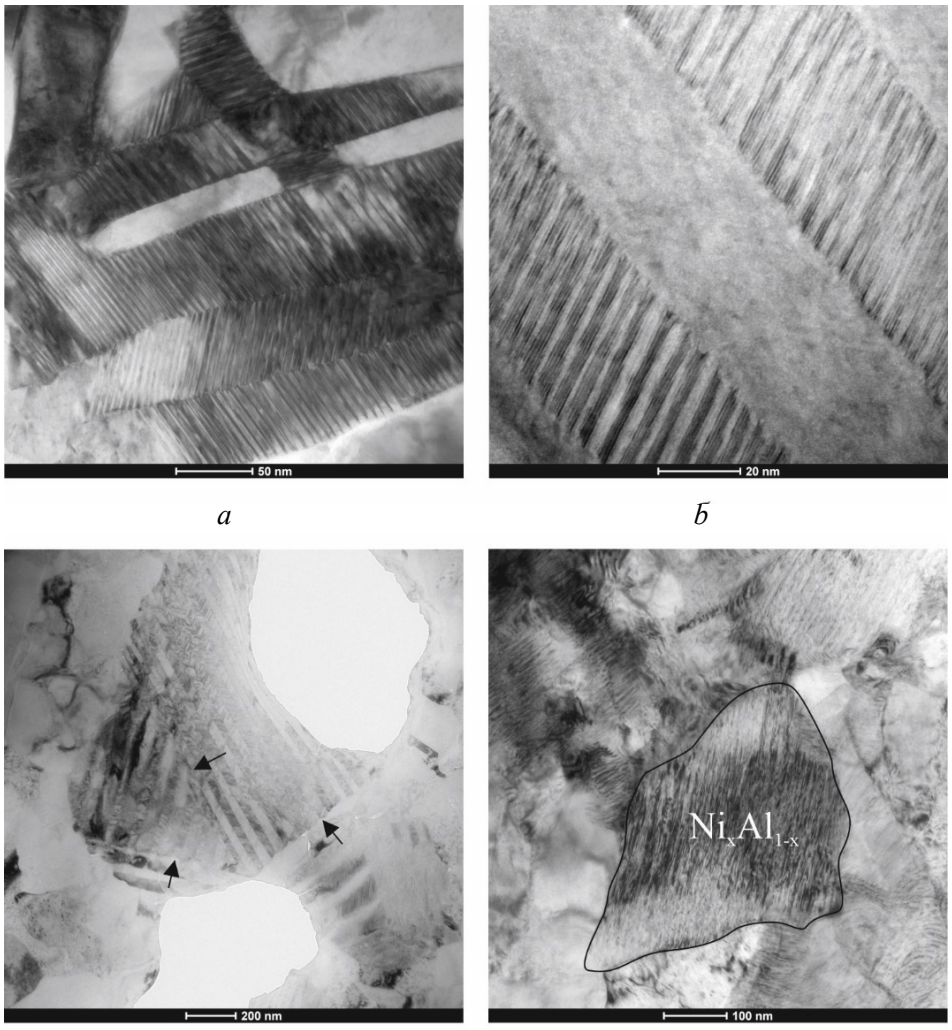

a *б*

c *d*

Fig. 4. Bright field *TEM* images of martensite:
a–c – lamellar martensite in coarse grains of Ni_xAl_{1-x}; *d* – lamellar martensite in fine grains of Ni_xAl_{1-x}

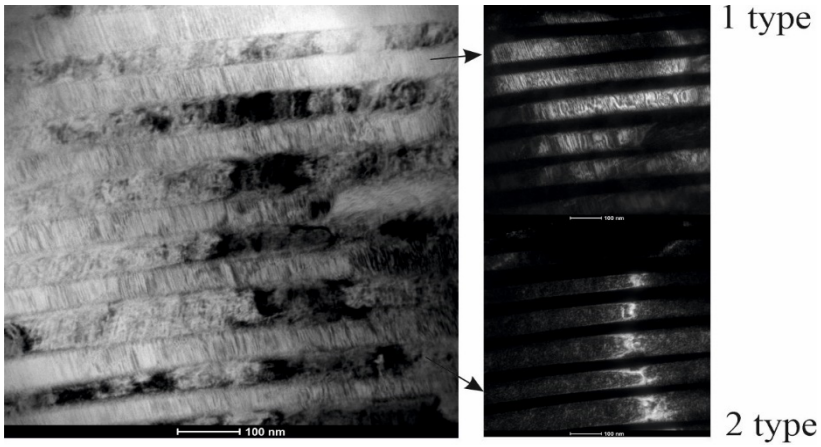

a *b*

Fig. 5. TEM image of martensite with different types of plates:
a – bright field image; *b* – dark field image

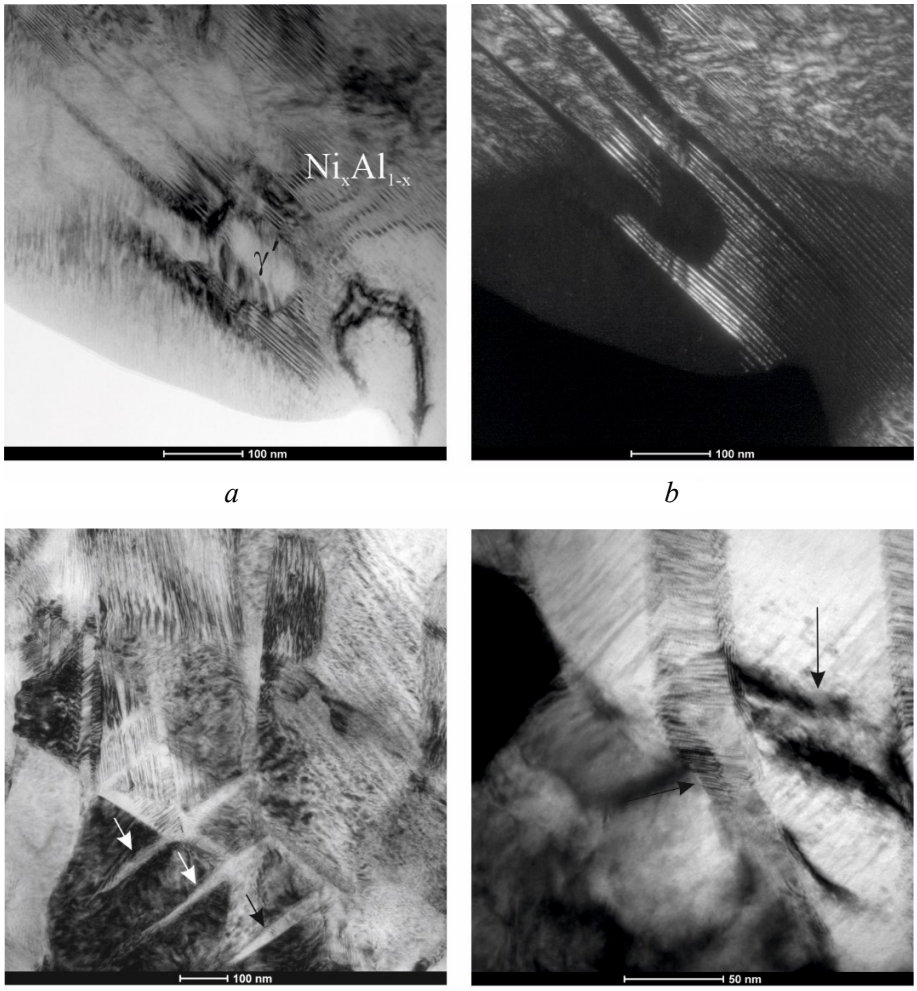

Fig. 6. Interaction of martensite with other phases:
a, b – collision of martensite plate with grain γ′-Ni_3Al; *c* – growth of martensite plates into grain; *d* – martensite plate deformation; *a*, *c*, *d* – bright field; *b* – dark field

It was shown above that the temperature of martensitic transformation in *Ni-Al* alloys is determined by the chemical composition of the material. Coating heating at 400–600 °C allows obtaining information about structural changes in the material. We do not observe any noticeable changes at lower heating temperatures. Fig. 7 demonstrates *TEM* images of the microstructure of *HV-APS* coatings after heating at *400* and *500* °C. According to structural studies, the beginning of the reverse transition of $\boldsymbol{L1_0}$ martensite to the ***B2*** structure is observed at 400 °C. In addition, a secondary phase in the form of elongated disks segregates along the boundaries of microtwins (Fig. 7, *a*). In some cases, only part of the martensite plate undergoes transformation. This can be explained by differences in the chemical composition within the same crystal. An increase in temperature to 500 °C leads to further decomposition of martensite plates and the growth of an already precipitated secondary phase (Fig. 7, *b*). The secondary phase in grains, where martensite has completely transformed, is oriented in one direction. The formation of the secondary phase is characteristic only for Ni_xAl_{1-x} grains and is absent in grains of the γ′-Ni_3Al phase (Fig. 7, *b*) and β-*NiAl* plates (fig. 7, *c*). The internal structure of β-*NiAl* plates is characterized by a relatively uniform distribution of dislocations. Finally, heating to these temperatures does not lead to any noticeable structural changes in small grains of the Ni_xAl_{1-x} phase (fig. 7, *d*).

A significant increase in the width of grain boundaries is observed in two-phase regions after heating at 600 °C (Fig. 8, *a*, *b*). The shape of the γ′-Ni_3Al and Ni_xAl_{1-x} grains approaches equiaxial, which indicates the occurrence of recrystallization processes. A growth of the secondary phase with increasing temperature

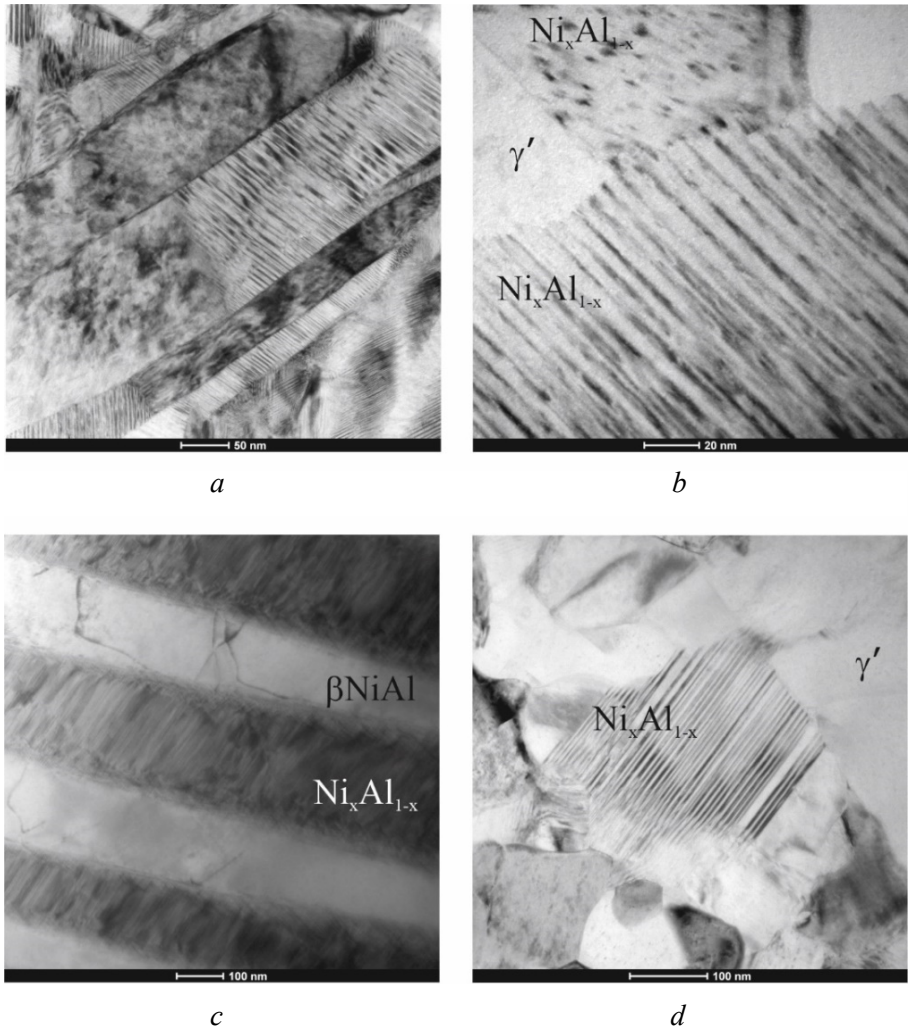

Fig. 7. Bright field images of coating structure after heating 400 (*a*, *c*, *d*) and 500 °C (*b*)

is not observed. The structure also contains martensite crystals in which the $\boldsymbol{L1_0 \rightarrow B2}$ transformation has completely occurred. Fig. 8, *c*, *d* shows bright-field and dark-field images of former martensite plates. Data of dark-field analysis confirms the presence of the secondary phase in former martensite plates, the chemical composition of which corresponds to the Ni_xAl_{1-x} phase (Fig. 8, *d*). The completely transformed plates are separated from each other by low-angle boundaries.

Conclusions

There are two types of particles in *HV-APS* coatings: with a dendritic and grain structure. The center of particles with a dendritic structure consists of the β-*NiAl* phase surrounded by a one-phase layer of the Ni_xAl_{1-x} phase and a layer of dendrites (Ni_xAl_{1-x}) with interdendritic space (γ'-Ni_3Al). Most of the coatings are particles with a grain structure (Ni_xAl_{1-x} and γ'-Ni_3Al grains).

Only Ni_xAl_{1-x} grains experience martensitic transformation when the particles are cooled. In the large grains, larger than 500 nm, martensite consists of plates in a twinned orientation relative to each other, while small grains are completely transformed into one microtwinning plate. In addition, there are grains in which martensite and β-phase plates alternated.

The collision behavior of martensitic plates is different. Thin plates at collision pass through each other and only the area of its intersection is rearranged. When a martensitic plate collides with an already formed γ′-Ni_3Al grain, the plate continues to transform without penetration. If martensitic plates were formed first, the γ′-Ni_3Al phase is formed around it. In addition, thin plates at collision with an obstacle can be deflected.

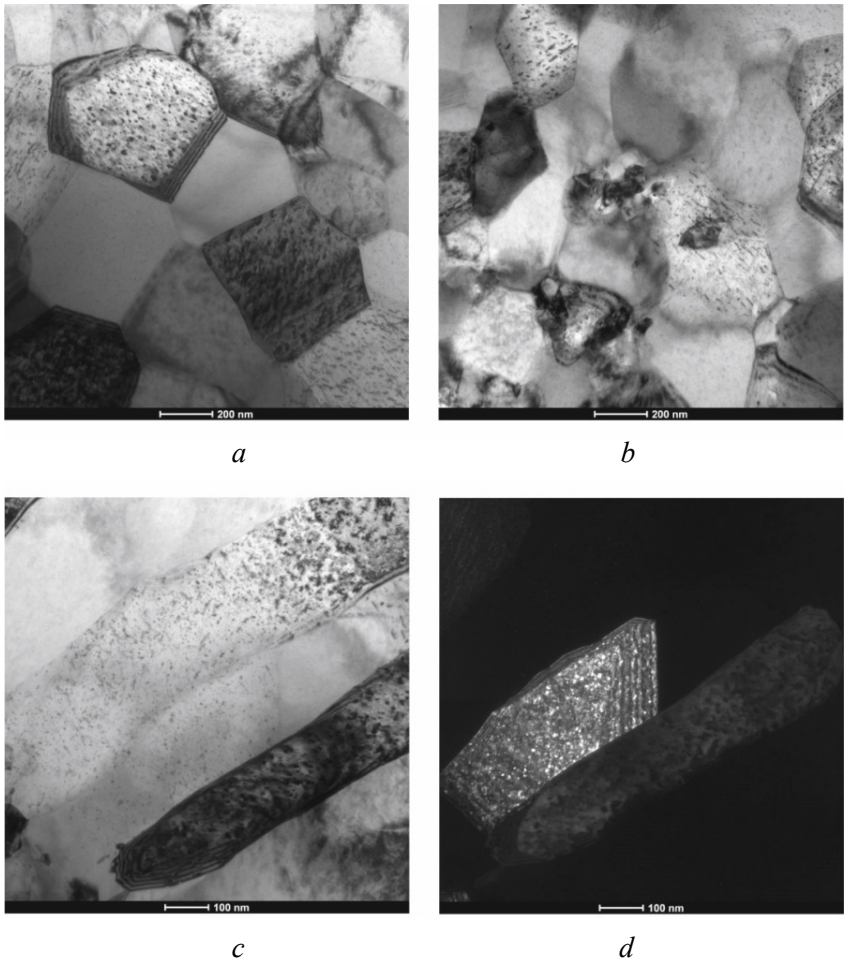

a *b*

c *d*

Fig. 8. TEM images of coating structure after heating 600 °C:
a, *b* – two-phase area; *c*, *d* – prior martensite plates; *a*, *b*, *c* – bright field;
d – dark field

When heated to 400 °C in large grains of Ni_xAl_{1-x}, the beginning of the reverse transition of $\boldsymbol{L1_0}$ martensite to ***B2*** structure with the secondary phase formation along microtwins is observed. No changes are observed in small grains of the Ni_xAl_{1-x} phase, γ′-Ni_3Al grains and β-*NiAl* plates. After heating to 600 °C, the shape of the γ'-Ni_3Al and Ni_xAl_{1-x} grains approaches equiaxial, which indicates the occurrence of recrystallization processes. The secondary phase is oriented in one direction in Ni_xAl_{1-x} grains. The martensite crystals in large grains are completely transformed into the ***B2*** structure, although it retained its orientation.

References

1. Bochenek K., Basista M. Advances in processing of NiAl intermetallic alloys and composites for high temperature aerospace applications. *Progress in Aerospace Sciences*, 2015, vol. 79, pp. 136–146. DOI: 10.1016/j.paerosci.2015.09.003.

2. Müller M., Enghardt S., Kuczyk M., Riede M., López E., Brueckner F., Marquardt A., Leyens C. Microstructure of NiAl-Ta-Cr in situ alloyed by induction-assisted laser-based directed energy deposition. *Materials & Design*, 2024, vol. 238, p. 112667. DOI: 10.1016/j.matdes.2024.112667.

3. Zhou L., Mehta A., Cho K., Sohn Y. Composition-dependent interdiffusion coefficient, reduced elastic modulus and hardness in γ-, γ′- and β-phases in the Ni-Al system. *Journal of Alloys and Compounds*, 2017, vol. 727, pp. 153–162. DOI: 10.1016/j.jallcom.2017.07.256.

4. Darolia R. Ductility and fracture toughness issues related to implementation of NiAl for gas turbine applications. *Intermetallics*, 2000, vol. 8 (9–11), pp. 1321–1327. DOI: 10.1016/S0966-9795(00)00081-9.

5. Li Y., Li C., Wu J., Wu Y., Ma Z., Yu L., Li H., Liu Y. Formation of multiply twinned martensite plates in rapidly solidified Ni_3Al-based superalloys. *Materials Letters*, 2019, vol. 250, pp. 147–150. DOI: 10.1016/j.matlet.2019.05.012.

6. Wang J., Qian J., Zhang X., Wang Y. Research status and progress of NiAl based alloys as high temperature structural materials. *Rare Metals*, 2011, vol. 30, pp. 422–426. DOI: 10.1007/s12598-011-0317-2.

7. Abuwarda N., Lopez A.J., Lopez M.D., Utrilla M.V. High temperature corrosion and wear behavior of HVOF-sprayed coating of Al_2O_3-NiAl on AISI 304 stainless steel. *Surface and Coating Technology*, 2019, vol. 359, pp. 35–46. DOI: 10.1016/j.surfcoat.2018.12.047.

8. Chi H., Pans M.A., Bai M., Sun C., Hussain T., Sun W., Yao Y., Lyu J., Liu H. Experimental investigations on the chlorine-induced corrosion of HVOF thermal sprayed Stellite-6 and NiAl coatings with fluidised bed biomass/anthracite combustion systems. *Fuel*, 2021, vol. 288, p. 119607. DOI: 10.1016/j.fuel.2020.119607.

9. Sadeghimeresht E., Markocsan N., Nylén P. A comparative study on Ni-based coatings prepared by HVAF, HVOF, and APS methods for corrosion protection applications. *Journal of Thermal Spray Technology*, 2016, vol. 25, pp. 1604–1616. DOI: 10.1007/s11666-016-0474-9.

10. Sadeghimeresht E., Markocsan N., Nylén P. Microstructural and electrochemical characterization of Ni-based bi-layer coatings produced by the HVAF process**.** *Surface and Coating Technology*, 2016, vol. 304, pp. 606–619. DOI: 10.1016/j.surfcoat.2016.07.080.

11. Mehmood K., Rafiq M.A., Durrani Y.A., Khan A.N. Effect of isothermal treatment on Ni_3Al coatings deposited by air plasma spraying system. *Archives of Metallurgy Materials*, 2018, vol. 63, pp. 277–283. DOI: 10.24425/118938.

12. Zhang L., Wang D., Liao X.-J., Chen R., Luo X.-T., Li C.-J. Study on the oxidation resistance mechanism of self-healable NiAl coating deposited by atmospheric plasma spraying. *Materials Degradation*, 2023, vol. 7, p. 62. DOI: 10.1038/s41529-023-00383-0.

13. Poliarus O., Morgiel J., Umanskyi O., Pomorska M., Bobrowski P., Szczerba M.J., Kostenko O. Microstructure and wear of thermal sprayed composite NiAl-based coatings. *Archives of Civil and Mechanicals Engineering*, 2019, vol. 19, pp. 1095–1103. DOI: 10.1016/j.acme.2019.06.002.

14. Mirche K.K., Pandey K.K., Pandey S.M., Keshri A.K. Microstructure and corrosion behavior of plasma-sprayed nanodiamond-reinforced NiAl nanocomposite coating. *Journal of Thermal Spray Technology*, 2023, vol. 32, pp. 1299–1310. DOI: 10.1007/s11666-023-01558-6.

15. Saltykov P., Cornish L., Cacciamani G. Al-Ni binary phase diagram evaluation. *MSI Eureka*. Ed. by G. Effenberg. MSI, 2004. Available at: https://materials.springer.com/msi/docs/sm_msi_r_20_010238_01 (accessed 21.08.2024).

16. Kositsyn S.V., Kositsyna I.I. Fazovye i strukturnye prevrashcheniya v splavakh na osnove monoalyuminida nikelya [Phase and structural transformations in the alloys based on monoaluminide of nikel]. *Uspekhi fiziki metallov = Progress in Physics of Metals*, 2008, vol. 9 (2), pp. 195–258. DOI: 10.15407/ufm.09.02.195.

17. Potapov P.L., Ochin P., Pons J., Schryvers D. Nanoscale inhomogeneities in melt-spun Ni-Al. *Acta Materialia*, 2000, vol. 48, pp. 3833–3845. DOI: 10.1016/S1359-6454(00)00188-9.

18. Potapov P.L., Song S.Y., Udovenko V.A., Prokoshkin S.D. X-ray study of phase transformations in martensitic Ni-Al alloys. *Metallurgical and Materials Transactions A*, 1997, vol. 28A, pp. 1133–1142. DOI: 10.1007/s11661-997-0279-z.

19. Schryvers D., Boullay P., Potapov P.L., Kohn R.V., Ball J.M. Microstructures and interfaces in Ni-Al martensite: comparing HRTEM observations with continuum theories. *International Journal of Solids and Structures*, 2002, vol. 39, pp. 3543–3554. DOI: 10.1016/S0020-7683(02)00167-1.

20. Kim S.H., Oh M.H., Wee D.M. Effects of ternary additions on the thermoelastic martensitic transformation of NiAl. *Metallurgical and Materials Transactions A*, 2003, vol. 34A, pp. 2089–2095. DOI: 10.1007/s11661-003-0273-z.

21. Schryvers D., Ma Y., Toth L., Tanner L. Electron microscopy study of the formation of Ni_5A1_3 in a $Ni_{62.5}A1_{37.5}$ B2 alloy. I. Precipitation and growth. *Acta Metallurgica et Materialia*, 1995, vol. 43 (11), pp. 4045–4056.

22. Schryvers D., Ma Y. The growth of Ni_5Al_3 in $L1_0$ martensite studied by in situ transmission electron microscopy and high resolution electron microscopy. *Journal of Alloys and Compounds*, 1995, vol. 221, pp. 227–234. DOI: 10.1016/0925-8388(94)01467-1.

23. Gong X., Peng H., Ma Y., Guo H., Gong S. Microstructure evolution of an EB-PVD NiAl coating and its underlying single crystal superalloy substrate. *Journal of Alloys and Compounds,* 2016, vol. 672, pp. 36–44. DOI: 10.1016/j.jallcom.2016.02.115.

24. Chen M.W., Glynn M.L., Ott R.T., Hufnagel T.C., Hemker K.J. Characterization and modeling of a martensitic transformation in a platinum modified diffusion aluminide bond coat for thermal barrier coatings. *Acta Materialia*, 2003, vol. 51, pp. 4279–4294. DOI: 10.1016/S1359-6454(03)00255-6.

25. Kornienko E., Gulyaev I., Smirnov A., Nikulina A., Ructuev A., Kuzmin V., Tuezov A. Microstructure and properties of Ni-Al coatings obtained by conventional and high-velocity atmospheric plasma spraying. *Results in Surfaces and Interfaces*, 2022, vol. 6, p. 100038. DOI: 10.1016/j.rsurfi.2022.100038.

Conflicts of Interest

The authors declare no conflict of interest.